MATERIALS SCIENCE

Helical coassembly enables full-color efficient circularly polarized light emission from carbon dots with high dissymmetry factors

Jinsui Li[1], Qinghua Tan[1], Jinyang Li[1], Wendi Qin[1], Chenhao Li[1], Qian Teng[1], Yuyue Yang[1], Yifeng Wang[1], Ye Cao[1], Yuchen Hu[1], Jibin Zhang[2], Fanglong Yuan[1]*

Printing materials with circularly polarized light (CPL) emission holds promise for flexible stereoscopic displays and multilevel anticounterfeiting solutions. However, a key challenge lies in developing printable CPL materials that exhibit both high photoluminescence quantum yield (PLQY) and luminescence dissymmetry factor (g_{lum}) values. In this study, we present the macroscopic and controllable production of efficient full-color CPL carbon dot (CDs) photonic paint materials. These printable CPL materials, consisting of heavy metal-free CDs as emitters, and liquid crystals as host matrices, are produced using a helical coassembly strategy. Our CPL systems based on CDs achieve high PLQY (more than 80%) and g_{lum} values (more than 1.4), with a figure of merit (a key performance indicator for CPL properties calculated by multiplying PLQY and glum) of 1.12, outperforming other CPL material systems. Furthermore, the full-color CDs-CPL is successfully used for printing flexible circularly polarized luminous patterns and multilevel anticounterfeiting features. This research provides insights into advanced CPL materials, highlighting their broad potential applications.

INTRODUCTION

Circularly polarized light (CPL) has unique properties such as optical rotatory power and angle independence, making it highly attractive for applications in anticounterfeiting (*1*–*3*), three-dimensional (3D) optical displays (*4*–*6*), and photoelectronic devices (*7*–*9*). CPL can be generated using a linear polarizer and a quarter-wave plate (QWP), but this approach leads to energy loss and requires additional optical components, hindering device integration (*10*). Now, conventional chiroptical materials such as organic molecules and metal complexes capable of producing CPL typically have luminescence dissymmetry factor (g_{lum}) values usually smaller than 0.1 (*11*–*14*). Quantum dots (QDs) are recognized as highly promising emitters for generating CPL owing to their exceptional optical properties. However, most well-developed QDs now rely on heavy metal–based systems, such as cadmium (Cd) and lead (Pb) halide perovskites. Moreover, the CPL performance of chiral QDs remains limited, with the g_{lum} values of Cd/Pb-based QDs falling far below satisfactory levels (*15*–*19*). For example, chiral CdSe@ZnS QDs incorporating l-/d-histidine ligands during ZnS shell growth have exhibited enhanced CPL with g_{lum} values of 10^{-2} (*15*). Further improvement has been achieved by embedding these QDs into inorganic chiral photonic crystals, increasing the g_{lum} value to 0.25 (*16*). In addition, core-shell perovskite QDs, consisting of a 2D chiral perovskite shell deposited onto an achiral 3D inorganic perovskite ($CsPbBr_3$) QD core, have demonstrated a g_{lum} value of 0.24 in electroluminescence (*17*). The combination of low g_{lum} values and the inherent toxicity of heavy metals have restricted the practical applications of these CPL-active QD materials. Consequently, there is an urgent demand for high-performance, eco-friendly QD alternatives that exhibit enhanced g_{lum} values to drive advancements in real-world applications within this field.

Chiral liquid crystals (CLCs), a type of quasi-1D photonic crystal, have been shown to achieve efficient CPL with g_{lum} values exceeding 10^{-1} by using their helical structures (*20*–*22*). However, current CPL-active CLC materials are limited to mobile phases and require confinement in layered devices or cell structures, restricting their application in flexible 3D displays and other versatile uses (*23*–*25*). In addition, the figure of merit (FM), which is a key performance indicator for evaluating the CPL properties of chiral materials, is calculated by multiplying the photoluminescence quantum yield (PLQY) by the g_{lum} values (*1*). To date, there are very few reports of CPL materials that achieve both high g_{lum} values and high PLQY. Therefore, there is an urgent need to develop printable CPL materials composed of CLCs and efficient light emitters that combine high PLQY with large g_{lum} values to unlock their full potential for diverse applications.

In recent years, carbon dots (CDs)—an emerging class of heavy metal-free QD materials—have emerged as promising candidates for next-generation high-performance light-emitting diode (LED) displays and lighting. Their potential stems from their excellent photo- and thermal stability, environmental friendliness, good solution processability, and adjustable bandgap emission (*26*–*32*). In the past few years, our group, along with collaborators, has developed a series of bright and efficient CDs with high PLQY and tunable fluorescence that spans the entire visible spectrum for LED display and lighting applications (*33*–*42*). In this work, we demonstrate the macroscopic and controllable production of efficient full-color circularly polarized luminescent photonic paint materials. These printable CPL materials, consisting of efficient heavy metal-free CDs as emitters and liquid crystals as host matrices, are produced using a helical coassembly strategy. We further encapsulate the CLC precursors and CDs (CDs-CLC) with a polymer shell to create solid-state CPL-active photonic paints (CDs-CPL), which exhibit intense CPL emission (*43*). By varying the emission colors of the CDs, we have successfully

[1]Key Laboratory of Theoretical and Computational Photochemistry of Ministry of Education, College of Chemistry, Beijing Normal University, Beijing, 100875, China. [2]Key Laboratory of Materials Physics of Ministry of Education, School of Physics, Zhengzhou University, Zhengzhou 450001, China.
*Corresponding author. Email: flyuan@bnu.edu.cn

achieved full-color and white-emissive CDs-CPL. Notably, the CDs-CLC core and CDs-CPL systems demonstrate high PLQY more than 80%, high g_{lum} values of 1.4 and 0.92, with corresponding high FM values of 1.12 and 0.75, surpassing other CPL material systems (table S1). In addition, CDs-CPL has been effectively used for printing circularly polarized luminous patterns and multilevel anticounterfeiting features. This work is poised to offer insights into the development of advanced CPL materials and holds promise for applications in information storage, encryption, anticounterfeiting, and flexible 3D displays.

RESULTS

Synthesis of the full-color CDs-CPL

The process for the macroscopic and controllable preparation of full-color CDs-CPL is illustrated in Fig. 1A. We began by ensuring that CLCs and CDs were uniformly assembled into a spiral superstructure to achieve intense CPL while also controlling the fluidity of the CDs-CPL structures. To this end, we used a confining helical coassembly approach. The CDs-CLC precursor mixtures were emulsified and coacervated with aqueous solutions of gelatin and acacia and then cross-linked for offline processing into structurally colored CDs-CPL with strong CPL emission (*43*, *44*). Specifically, we used the chiral dopants S5011 and R5011 (fig. S1), known for their high helical twisting power, to form helical superstructures within the nematic liquid crystal host E7, demonstrating effectiveness across a wide temperature range. Typical planar textures are distinctly visible in the polarized optical microscopy (POM) images of liquid crystal cells composed of E7 and chiral dopants, highlighting the characteristic organization of a chiral nematic liquid crystal phase with its helical axis oriented perpendicular to the substrate (fig. S2) (*45*, *46*). CDs, which are compatible with CLCs, were incorporated to produce CPL with the opposite handedness of the helical superstructures, due to the photonic bandgap (PBG) effect. We achieved dispersion of the CLC droplets using natural polymer acacia and gelatin as emulsifiers, carefully controlling the pH to ensure that the gelatin-acacia coacervates fully covered the CLC droplets. After emulsification and coacervation, gelatin reacted with formaldehyde to form an amine-aldehyde condensation network, cross-linking the gelatin molecules into a firm shell. The final CDs-CPL product was obtained through further centrifugation and purification under ambient conditions. Encapsulating the CDs-CLC cores with a polymer shell physically restricts the mobility of liquid crystal molecules, thereby stabilizing the CPL emission. In addition, it ensures uniform dispersion of CDs and prevents aggregation-induced quenching, effectively transforming the liquid system into a solid-compatible material.

We adjusted the PBGs of CLCs across a wide wavelength range from 400 to 700 nm by varying the weight ratios of R/S5011 chiral dopant to E7 liquid crystal. Specifically, as the weight ratios of chiral dopant to E7 liquid crystals decreased from 3.4 to 2.1%, the reflection spectra exhibited a notable red shift, moving from the ultraviolet (UV)–blue region to the red near-infrared region (Fig. 1B). This tunability of PBGs is demonstrated by the varying structural colors of the liquid crystal cells across the entire visible spectra region (Fig. 1C). We used these tunable PBGs to prepare CDs-CLC cores that correspond to the fluorescence emission wavelengths of blue, green,

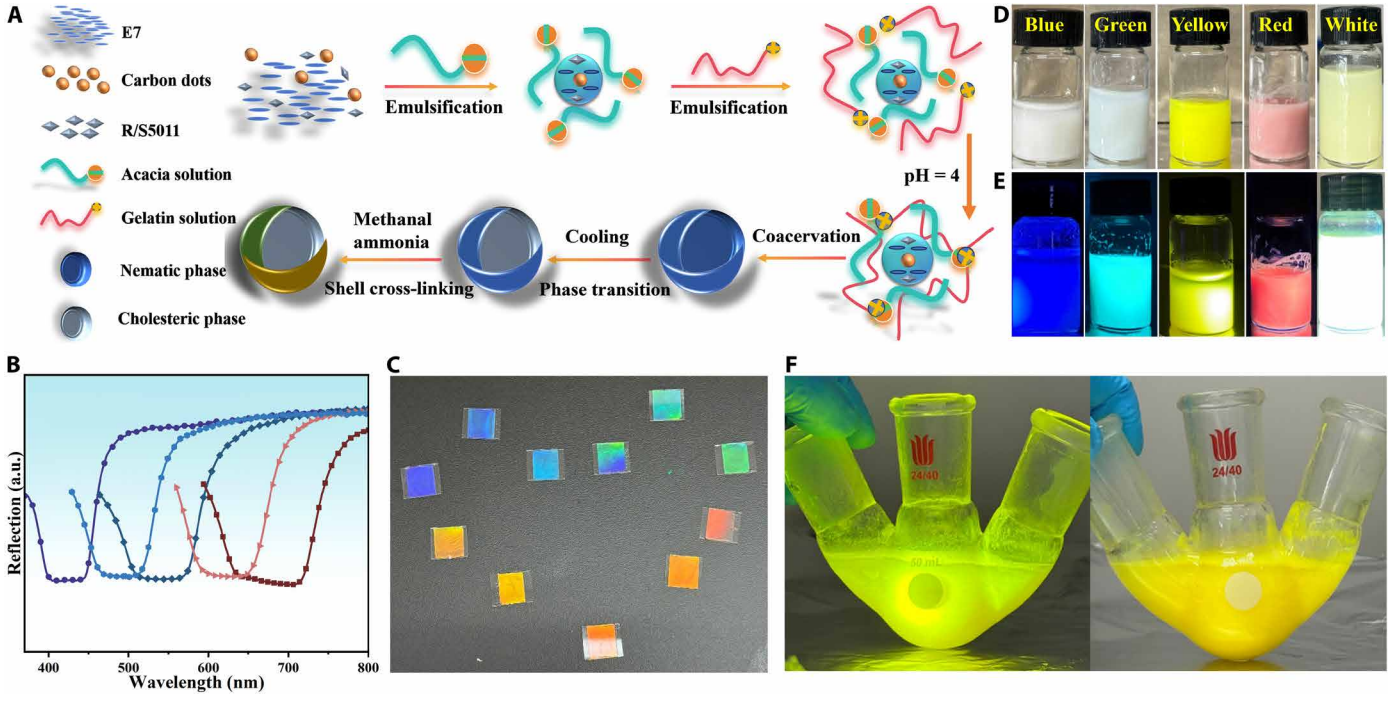

Fig. 1. Schematic illustration of the synthesis of the full-color CDs-CPL. (**A**) Schematic diagram of the preparation process of CDs-CPL. (**B**) Reflection spectra of CLCs with varying chiral R/S5011 doping ratios. From left to right, the weight ratios of the chiral dopant to E7 liquid crystals are 3.4, 3, 2.7, 2.3, and 2.1%, respectively. (**C**) Photographs of the liquid crystal cells with different PBGs, showing different appearance colors from blue to red, prepared by varying the weight ratios of the chiral dopant to E7 liquid crystals. Photographs of the full-color (blue, green, yellow, red, and white) CDs-CPL under natural light (**D**) and ultraviolet (UV) light (**E**). (**F**) Photographs of the yellow-CDs-CPL prepared in large quantities under natural light (right) and UV light (left). a.u., arbitrary units.

yellow, and red CDs. Consequently, full-color CDs-CPL with blue, green, yellow, red, and white light emission can be produced by encapsulating the CDs-CLC cores with a polymer shell. The full-color CDs-CPL are well-dispersed in water and are printable (Fig. 1D), exhibiting bright blue, green, yellow, red, and white light emission under UV light (Fig. 1E). Furthermore, the CDs-CPL can be manufactured in large quantities, which is essential for their broad potential applications (Fig. 1F).

Optical and structural characterization of the full-color CDs-CPL

For comparison, we have also prepared control CPL samples without incorporating CDs into CLC precursors using the same preparation process. These control samples exhibited violet light emission, which originated from the E7 liquid crystals. Bright-field microscopy images revealed that the control violet CPL sample, as well as the blue-, green-, yellow-, and red-CDs-CPL, is uniformly dispersed as microspheres (Fig. 2, A, C, E, G, and I). Fluorescence microscopy images demonstrated the violet, blue, green, yellow, and red emission color from the control sample and the full-color CDs-CPL (Fig. 2, B, D, F, H, and J). By increasing the magnification, the bright-field images provided a clear view of the complete and uniform microsphere structure, confirming the effectiveness of the complex condensation method in limiting the fluidity of the CDs-CLC core (Fig. 2K). In addition, POM images displayed a classic Maltese cross pattern, indicating that the CDs-CPL have a centrosymmetric parallel orientation with a radial distribution of helical axes (Fig. 2L and fig. S3) (*43*). Compared to the texture, a typical optical pattern observed in planar-aligned chiral nematic liquid crystals, the Maltese cross pattern is a distinctive optical feature that emerges when liquid crystal molecules adopt a radial alignment within a spherical or droplet-like confinement (*47*). This pattern arises from the interplay between homeotropic anchoring at the curved interface, which forces molecules to align perpendicular to the surface and the intrinsic helical structure of CLCs. Variations in POM textures and the Maltese cross pattern can be attributed to the complex interaction between surface anchoring effects and the inherent helical ordering within the microcapsules.

The control CPL sample, prepared without CDs, exhibits violet light emission peaking at 395 nm. In contrast, after incorporating CDs with various emission colors—blue, green, yellow, and red—CDs-CPL display emission peaks at 442, 498, 560, and 634 nm, respectively (Fig. 3A). Moreover, all the CDs-CPL samples can be excited over a wide wavelength range, and the position of the maximum emission peaks remains almost unchanged with varying excitation wavelengths (figs. S4 and S5). It is worth noting that, compared to CDs in a diluted solution, the solid-state blue-CDs-CPL sample undergoes a certain degree of aggregation due to its higher concentration in the solid state. This aggregation results in a further broadening of the main emission peak and the emergence of a more pronounced shoulder peak (fig. S6). Notably, no violet light emission from the control sample was observed in the CDs-CPL. In addition, the emission colors of the CDs-CPL, including cyan, pink, yellow-green, and orange, can be widely tuned by mixing different

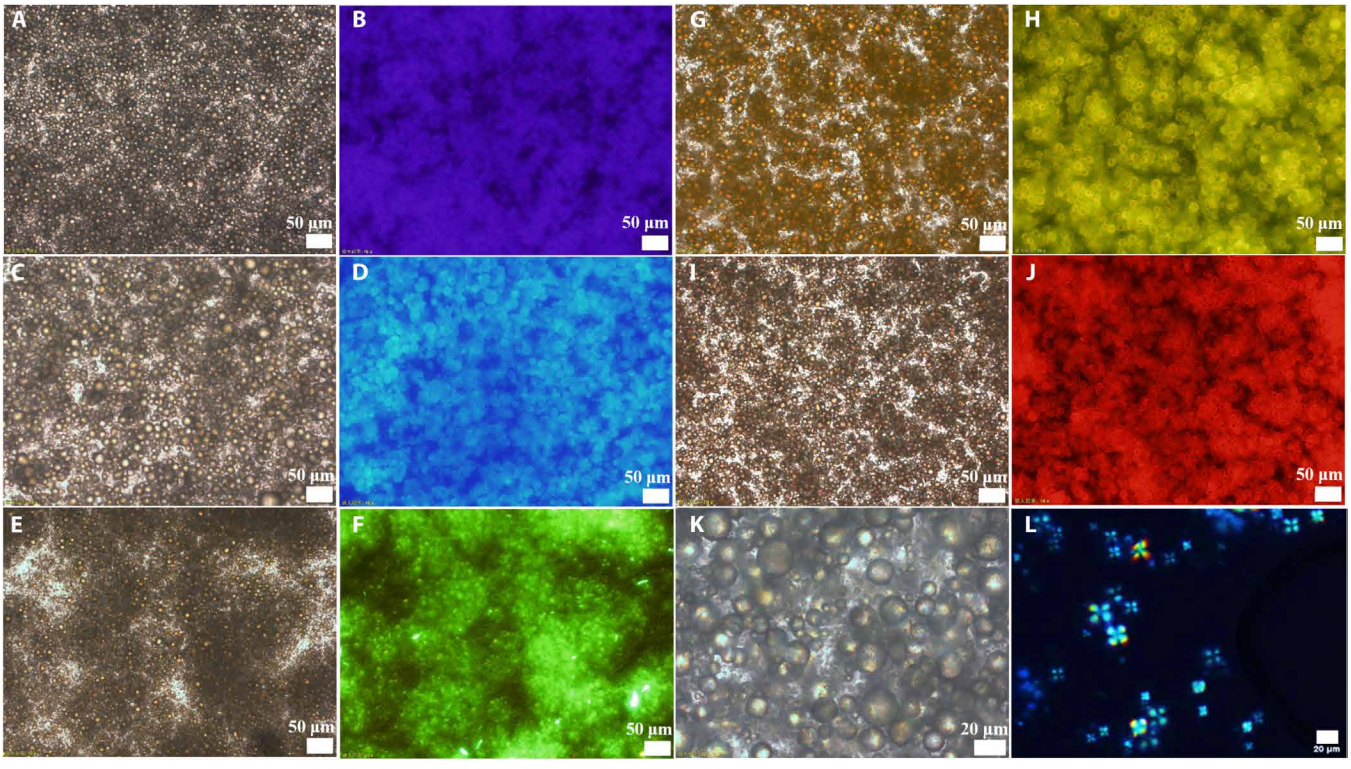

Fig. 2. Micromorphology of the full-color CDs-CPL. Bright-field microscopy images of the control violet-CPL sample without the incorporation of CDs (**A**), blue- (**C**), green- (**E**), yellow- (**G**), and red- (**I**) CDs-CPL samples in the transmission mode and corresponding fluorescence microscopy images of the control violet-CPL sample (**B**), blue- (**D**), green- (**F**), yellow- (**H**), and red- (**J**) CDs-CPL samples. Scale bars, 50 μm. The enlarged bright-field optical microscopy image (**K**) and POM image (**L**) of blue-CDs-CPL. Scale bar, 20 μm.

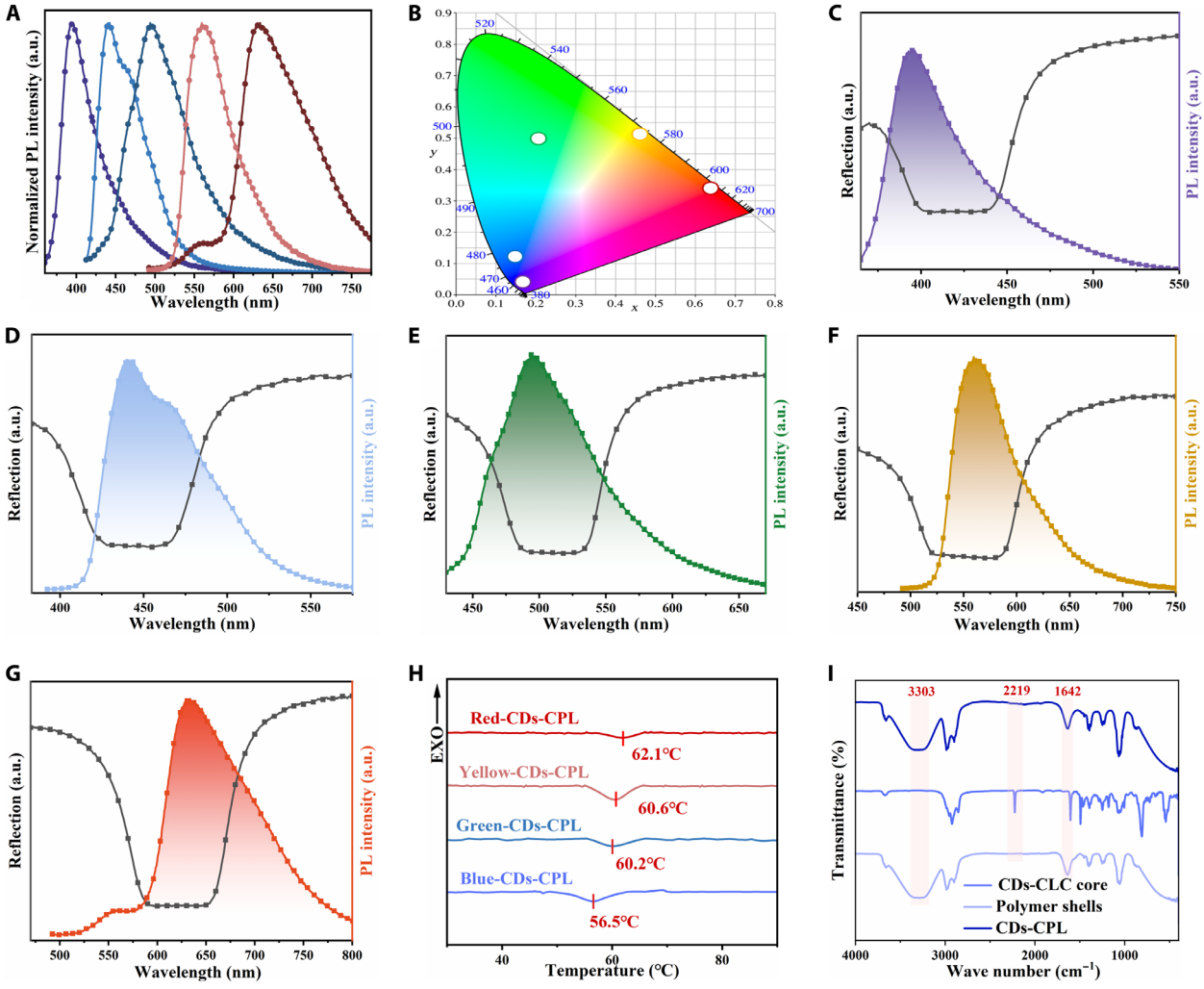

Fig. 3. Optical and structural characterization of the full-color CDs-CPL. (**A**) Normalized PL spectra of the control violet-CPL sample without the incorporation of CDs, blue-, green-, yellow-, and red-CDs-CPL samples. (**B**) 1931 CIE chromaticity coordinates corresponding to PL spectra of the CPL samples with different emission color. Reflection spectra of CLCs with chiral dopant to E7 liquid crystal weight ratios of 3.6% (**C**), 3.4% (**D**), 3% (**E**), 2.7% (**F**), and 2.3% (**G**) (black lines), along with their corresponding emission spectra of the control violet-CPL (C) and CDs-CPL samples [(D) to (G)]. (**H**) The DSC curves of CDs-CPL from 25° to 100°C in a nitrogen atmosphere. (**I**) The FTIR spectra of polymer shells, CDs-CLC core, and CDs-CPL. PL, photoluminescence.

CDs-CPL. For example, by blending blue- and yellow-CDs-CPL with different weight ratios, we achieved white-emissive CDs-CPL ranging from cold white to warm white (fig. S7). We calculated the chromaticity of the full-color CDs-CPL and plotted the results on the CIE 1931 chromaticity diagram (Fig. 3B). The chromaticity of the full-color CDs-CPL samples spans a broad range. According to Glassman's law, a wide spectrum of colors can be obtained by mixing different colors of CDs-CPL in appropriate proportions. To achieve high g_{lum} values for the CDs-CPL samples, the PBGs of the CLCs must align well with the emission spectra of the CDs. In our hybrid system, the PBGs are finely tuned by adjusting the weight ratio of the chiral dopant to the nematic liquid crystal. We varied the S/R5011 to E7 ratio to 3.6, 3.4, 3, 2.7, and 2.3% to achieve the desired PBGs that match the violet, blue, green, yellow, and red emission spectra (Fig. 3, C to G). The emission peaks of the CDs are predominantly within the PBG, although some spectral regions extend beyond it. This is primarily due to the relatively large full width at half maximum of the CDs' emission spectra compared with that of the reflection spectra.

Figure 3H shows a prominent endothermic peak in the differential scanning calorimetry (DSC) curve of CDs-CPL upon heating. This peak, corresponding to the anisotropy-to-isotropy phase transition (clearing point), decreases from 62.1° to 56.5°C as the weight ratio of chiral dopants increases from 2.3 to 3.4% (corresponding to red-, yellow-, green-, and blue-CDs-CPL). This decrease is possibly due to the higher chiral dopant content disrupting intermolecular interactions within the liquid crystal, thereby reducing the thermal stability of the mesophase. A similar trend is also observed in the CDs-CLCs (fig. S8). Figure 3I presents the Fourier transform infrared (FTIR) spectroscopy results for CDs-CPL, the individual polymer shells, and the CDs-CLC cores. Strong absorption peaks at 3303 cm^{-1} (O—H and N—H) and 1642 cm^{-1} (C═O) are associated with both the CDs-CPL and the polymer shells. Conversely, the adsorption peak at 2219 cm^{-1} (C≡N) is unique to the CDs-CLC cores, indicating

that the polymer shell does not affect the spatial distortion of the cholesteric helicoid.

CPL properties of the full-color CDs-CPL

The CPL and circular dichroism properties of control CLCs, CDs-CLC cores, and CDs-CPL have been extensively studied. The CLCs, which consist of liquid crystals E7 and chiral dopants R/S5011, exhibit an exceptionally large g_{lum} value of 1.82 (Fig. 4A). This value is remarkably close to the theoretical maximum g_{lum} value of 2, highlighting their notable potential as chiral host matrices for inducing efficient CPL from CDs. Even after incorporating CDs into the CLCs, the CDs-CLCs maintain high g_{lum} values exceeding 1.4 (figs. S9 and S10). The circular dichroism spectra for the blue-, green-, yellow-, and red-CDs-CLCs show very large circular dichroism values above 30,000 mdeg, with a noticeable red-shift from the blue to the red region, like the tunable PBGs across the whole visible-light regime by precise control of the weight ratios of R/S5011 to E7 liquid crystals (fig. S11). To verify the CPL characteristics of the CDs-CPL, we first measured the light transmittance using a QWP and a rotated analyzer. The QWP converts the CPL emitted from the CDs-CPL into linearly polarized light, which can be easily detected by the linear analyzer. As illustrated in Fig. 4 (B and C), we used blue- and yellow-CDs-CPL as examples. The left-handed and right-handed CPL emitted by the CDs-CPL were converted into linearly polarized light with orthogonal polarization planes. The results demonstrated the excellent circular polarization characteristics of the emissions from the CDs-CPL (fig. S12).

Furthermore, we evaluated the CPL performance of the CDs-CPL using a CPL spectrometer under ambient conditions, with excitation provided by a Xe lamp coupled to a monochromator. As shown in Fig. 4D, we observed strong mirror-symmetric CPL responses near the PL peaks of the CDs-CPL. Specifically, the left-handed CDs-CPL exhibited a negative CPL sign, while the right-handed CDs-CPL showed a positive CPL sign, due to the suppression of the CPL component with the same handedness as the chiral medium helix (figs. S13 to 15). All full-color CDs-CPL samples displayed high g_{lum} values greater than 0.74, with the control violet CPL and blue-CDs-CPL samples achieving g_{lum} values of 0.94 and 0.92, respectively (Fig. 4E). These high g_{lum} values can be attributed to the uniform morphology of the CDs-doped CLCs and the reduced scattering effects, which contribute to a highly ordered helical arrangement and a well-defined PBG, thereby enhancing the coupling between the CLCs and CDs. We firmly believe that further precise optimization of the alignment between the PBG and the emission spectra in future studies could lead to even greater enhancements in CPL performance. In addition, the CDs-CLC core and CDs-CPL systems demonstrated high PLQYs of more than 80% (fig. S16), with corresponding FM values of 1.12 and 0.75, surpassing other CPL material systems (table S1).

To investigate the chirality of CDs-CPL, we analyzed their circular dichroism spectra, which exhibited both positive and negative signals with large circular dichroism values (figs. S17 and S18). The reflection color of CDs-CPL results from Bragg reflection combined with the CD properties imparted by their periodic helical superstructures. For instance, right-handed CDs-CPL can selectively reflect

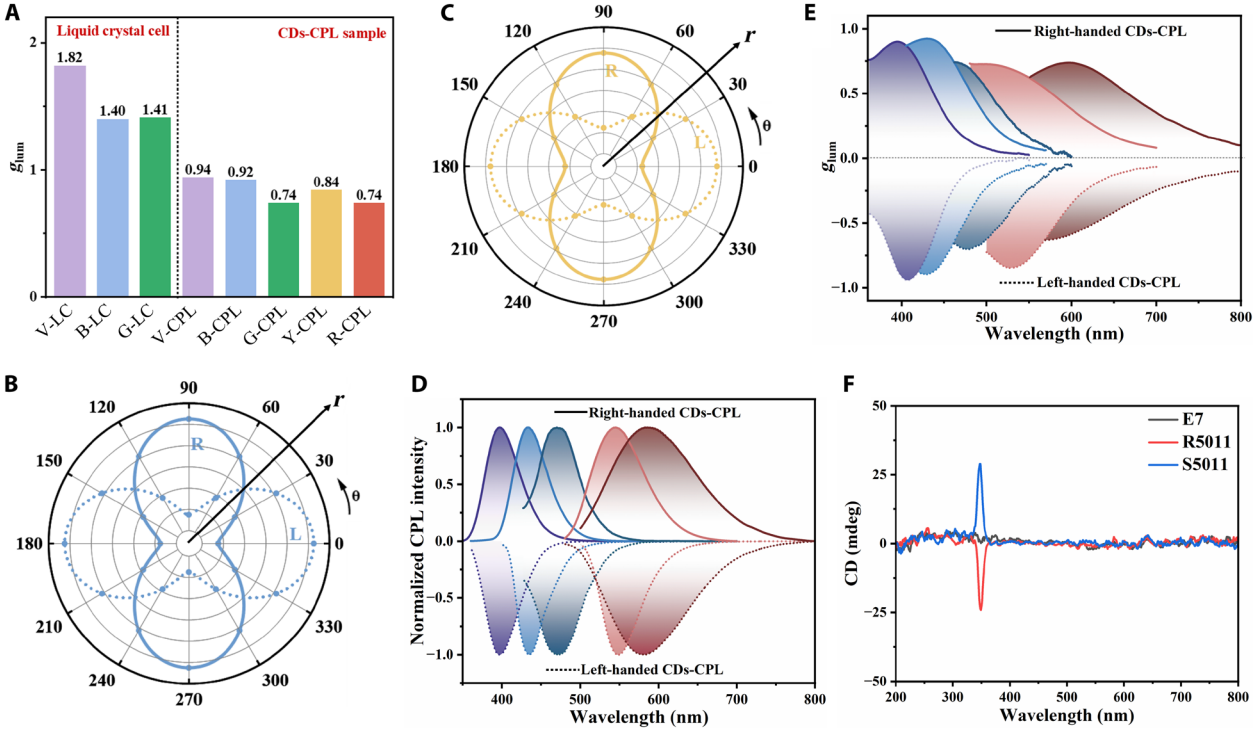

Fig. 4. CPL properties of the full-color CDs-CPL. (**A**) Bar charts of g_{lum} values of liquid crystal cells of control CLCs (V-LC), CDs-CLC core (B-LC and G-LC), and CDs-CPL (B-, G-, Y-, and R-CPL). Emission intensity of blue- (**B**) and yellow- (**C**) CDs-CPL as a function of polarization angle, where θ represents the transmission angle and *r* refers to the transmittance. The solid (dashed) curves correspond to right (left)–handed materials. (**D**) Normalized CPL spectra of CPL samples with different emission colors. (**E**) Calculated g_{lum} values corresponding to the CPL spectra of CPL samples with different emission colors. (**F**) Circular dichroism spectra of E7 liquid crystal and R/S5011, each measured separately in dichloromethane solution.

right-handed CPL, while left-handed CPL is transmitted and vice versa. Because of this PBG suppression, CDs-CPL can emit CPL opposite to their spiral superstructures. In contrast, single-component E7 and CDs dissolved in dichloromethane exhibit no noticeable circular dichroism signal (figs. S19 and S20), as their molecular structures are achiral and lack intrinsic circularly polarized absorption. However, R/S5011, being inherently chiral, displays a distinct yet relatively weak circular dichroism signal around 350 nm when measured in dichloromethane, with R5011 and S5011 exhibiting nearly opposite circular dichroism signals (Fig. 4F). This observation underscores that the strong circular dichroism signals observed in CDs-CPL across the broad visible region originate from their spiral superstructures induced by chiral dopants. Moreover, the circular dichroism and CPL spectra of CDs-CPL samples, measured at different rotation angles, exhibit no obvious variations, suggesting minimal influence from linear dichroism and linear birefringence (figs. S21 and S22).

Luminous patterns and multilevel anticounterfeiting of CDs-CPL

The solution-processible and printable full-color CDs-CPL, featuring both high QY and high dissymmetry factors, have promising applications across a range of fields, including information encryption, anticounterfeiting, 3D displays, photoelectronic devices, circularly polarized lasers, and asymmetric catalysis. The fluidic nature and solution processibility of CDs-CPL, along with their adhesive properties, allow producing large-scale customized graphics or coatings on various substrates through printing techniques. We used the optimized full-color CDs-CPL to directly print the text "CPL" and "BNU" on substrates using dispensing printing. As anticipated, the structural colors are not dependent on the angle of the text, and these texts emit bright CPL under UV irradiation. Moreover, the printing process does not require highly smooth surfaces and can be applied to flexible substrates. We chose PET fabric for its high strength and good elasticity and demonstrated the production of circularly polarized luminescent flexible textiles in blue, green, yellow, red, and white using dispensing printing (Fig. 5A).

Given the distinct CPL of right-handed and left-handed CDs-CPL, we integrated them into a multilevel anticounterfeiting system by incorporating them into a quick response (QR) code. As shown in Fig. 5B, the storage and positioning zones of the QR code are coated with left-handed and right-handed CDs-CPL, respectively. This multilevel anticounterfeiting system produces labels that remain invisible until exposed to UV light (365 nm) (Fig. 5C). Under UV illumination, the QR code becomes clearly visible, allowing for seamless scanning and reading with a mobile phone (Fig. 5D). This innovative approach establishes a robust first-level anticounterfeiting system based on the unique PL characteristics of the CDs-CPL. Furthermore, when the QR code is illuminated with UV light and scanned through a circular polarizer, an intriguing effect occurs. The brightness of the right-handed CDs-CPL in the positioning area selectively diminishes, creating a noticeable contrast between light and dark regions (Fig. 5E). As a result, the QR code becomes unrecognizable, adding an additional layer of security (Fig. 5F). This underscores the effectiveness of the highly efficient CPL from

Fig. 5. CDs-CPL for printing circular polarization luminous patterns and implementing multilevel anticounterfeiting. (**A**) Dispensing printed CPL and BNU circularly polarized luminous patterns on flexible PET fabric using full-color CDs-CPL. (**B**) Custom QR code creation. (**C** and **D**) First-level anticounterfeiting process of CDs-CPL based on PL characteristics. (**E** and **F**) Secondary anticounterfeiting process of CDs-CPL based on CPL characteristics.

CDs-CPL in strengthening anticounterfeiting systems. Our findings highlight the promising potential of chiral CDs-CPL in advancing multilevel security solutions, where their unique optical properties facilitate effective anticounterfeiting measures and provide robust deterrents against unauthorized replication or tampering.

DISCUSSION

In summary, we have successfully achieved controllable, large-scale production of full-color CDs-CPL by encapsulating CDs-doped CLCs in polymer shells through a confining helical coassembly strategy. Our CD-based CPL systems exhibit impressive PLQY (more than 80%) and exceptional g_{lum} values (more than 1.4), with a record-high FM of 1.12, surpassing other CPL material systems. These CDs-CPL materials are suitable for printing customized graphics on flexible PET fabrics and for applications in optical anticounterfeiting and intelligent information encryption. We anticipate that these advanced CDs-CPL materials will foster an exciting approach to next-generation flexible and wearable 3D display device applications.

MATERIALS AND METHODS

Materials

The chemicals listed below are readily available from commercial purchase and were used without further purification. The nematic liquid crystal host E7 ($n = 1.747$, $T_c = 60$°C) and the chiral dopants R/S5011 were purchased from Shijiazhuang Yesheng Chemical Technology Co. Gelatin is purchased from Sinopharm Chemical Reagent Co. Ltd. Dichloromethane, acetic acid (99%), and sodium hydroxide are all purchased from Beijing Innochem Science & Technology Corp. Arabic gum and formaldehyde solution (37 to 40% in water) are purchased from Adamas-Beta.

Preparation of CDs

The CDs were prepared following the methods reported in our previous works (*35*, *38*, *41*, *42*). For example, the red CDs were synthesized as follows: 2,5-dihexyloxybenzene-1,4-dialdehyde (60 mg) and 1,4-phenylenediacetonitrile (28 mg) were dissolved in ethanol (10 ml) and ultrasonically dispersed for 5 min. Subsequently, 1 ml of NaOH solution (3 mg/ml) was added to the reaction mixture, which was then transferred to a 25-ml capacity polytetrafluoroethylene–lined reactor. The mixture was heated in a drying oven at 150°C for 2 hours. After the reaction, the crude products were washed three times each with water, ethanol, and acetone using centrifugal separation. Last, the samples were dried in a vacuum oven at 60°C, yielding the red CDs. The yellow CDs were synthesized using a similar procedure, except that 2,5-dihexyloxybenzene-1,4-dialdehyde (60 mg) and 1,4-phenylenediacetonitrile (28 mg) were replaced with 2,5-dihexyloxybenzene-1,4-dialdehyde (50 mg) and 2-naphthylacetonitrile (50 mg).

Preparation of liquid crystal cell

Following procedures previously described in (*1*), silica microspheres (25.0 μm) were uniformly dispersed in a UV-curable adhesive using ultrasonic dispersion. The resulting mixture was placed between two glass sheets, which were then pressed together and exposed to UV light for approximately 30 s, ensuring complete adhesion. A pipette was used to extract 20 μl of the CDs-CLC core precursors, which contained the nematic liquid crystal host E7, chiral dopants R/S5011, and different CDs with various emission colors. This precursor solution was subsequently introduced into the liquid crystal cell by capillary action.

Preparation of CDs-CLC core

First, we modulated the PBG by mixing E7 with chiral dopants R/S5011 at weight ratios of 3.4, 3.0, 2.7, and 2.3%. These tunable PBGs were used to prepare CDs-CLC cores corresponding to the fluorescence emission wavelengths of blue, green, yellow, and red CDs, respectively. The CDs were added at a 1% weight ratio. The nematic liquid crystals, chiral dopants, and CDs were dispersed in dichloromethane and subjected to 5 min of ultrasonic treatment to form a uniform solution. After evaporating the solvent in a drying box, the resulting mixture was obtained as the CDs-CLC core precursors. A control violet CLC core precursor was prepared by mixing E7 with a 3.6% weight ratio of chiral dopants R/S5011, dispersing it in dichloromethane, and evaporating the solvent in the same manner.

Preparation of CDs-CPL

First, we homogenized the obtained CDs-CLC core precursors with a 2.0 wt % acacia solution for 30 min at 60°C using a high-speed emulsifier (HUXI, HR-6B) to create an emulsion (CDs-CLC core to acacia solution weight ratio of 1:25). Next, a 2.0 wt % gelatin solution was added, and the mixture was emulsified under the same conditions for an additional 30 min. The pH was then adjusted to 4 by adding acetic acid, followed by condensation at 60°C for 1 hour. Once the emulsion was cooled to 0°C in an ice water bath, formaldehyde solution was added and allowed to cure for 30 min (*43*). Sodium hydroxide was then added to adjust the pH to 8 to 9. Last, the sample was washed and centrifuged with deionized water three times to obtain the final product.

Optical and structural characterization

UV-visible absorption and reflection spectra were measured using a UV 2600. Fluorescence spectra were measured by a fluorescence spectrometer (HORIBA Fluorolog-3). Scanning electron microscopy was conducted using a Hitachi SU 8010 under a voltage of 5 kV. The absolute QY was obtained using a HAMAMATSU C11347. The thermogravimetric curves were measured by a NETZSCH STA 449F5 heated from 30° to 800°C at a ramp rate of 10°C/min, under a nitrogen flux of 100 ml/min. The DSC curves were measured by a differential scanning calorimeter (METTLER TOLEDO DSC-1). Circular dichroism and CPL spectra were measured by a JASCO J-1500 spectrophotometer and a JASCO CPL-300 spectrophotometer, respectively. Fluorescence microscopy images were obtained using an upright fluorescence microscope (Olympus, IX71) under the excitation of a mercury lamp. POM images are measured by an upright polarizing microscope (Olympus, BX53). The FTIR spectrum was measured with an FTIR spectrometer (IRAffinity-1).

Dispensing printing and multilevel anticounterfeiting applications of CDs-CPL

We used a pneumatic extrusion-type microelectronic printer (MP1100, Prtronic, China) with programmable temperature and pressure control for pattern printing. For dispensing, the optimized CDs-CPL was loaded into a 3-ml syringe fitted with a 160-μm dispensing needle. The release of the CDs-CPL was precisely controlled by adjusting the printing speed and pressure, allowing for complete customization of all patterns using the printer's integrated drawing software. Information patterns were prepared in two steps: First, CDs-CPL materials

were filled into customized pattern templates; then, we leave the pattern at room temperature for 1 hour to obtain a planar pattern in the shape of a 2D code.

Supplementary Materials

This PDF file includes:

Figs. S1 to S22
Table S1
References

REFERENCES AND NOTES

1. Q. Guo, M. Zhang, Z. Tong, S. Zhao, Y. Zhou, Y. Wang, S. Jin, J. Zhang, H.-B. Yao, M. Zhu, T. Zhuang, Multimodal-responsive circularly polarized luminescence security materials. *J. Am. Chem. Soc.* **145**, 4246–4253 (2023).
2. D.-Y. Liu, H.-Y. Li, R.-P. Han, H.-L. Liu, S.-Q. Zang, Multiple stimuli-responsive luminescent chiral hybrid antimony chlorides for anti-counterfeiting and encryption applications. *Angew. Chem. Int. Ed. Engl.* **62**, e202307875 (2023).
3. C. Xue, Y. Jiang, H.-X. Wang, C. Du, L. Xu, T. Li, M. Liu, Excitation-dependent circularly polarized luminescence from helical assemblies based on tartaric acid-derived acylhydrazones. *Angew. Chem. Int. Ed. Engl.* **61**, e202205633 (2022).
4. Y. Sang, J. Han, T. Zhao, P. Duan, M. Liu, Circularly polarized luminescence in nanoassemblies: Generation, amplification, and application. *Adv. Mater.* **32**, e1900110 (2020).
5. Y. Wu, M. Li, Z. Zheng, Z.-Q. Yu, W.-H. Zhu, Liquid crystal assembly for ultra-dissymmetric circularly polarized luminescence and beyond. *J. Am. Chem. Soc.* **145**, 12951–12966 (2023).
6. X. Zhan, F.-F. Xu, Z. Zhou, Y. Yan, J. Yao, Y. S. Zhao, 3D laser displays based on circularly polarized lasing from cholesteric liquid crystal arrays. *Adv. Mater.* **33**, e2104418 (2021).
7. D.-W. Zhang, M. Li, C.-F. Chen, Recent advances in circularly polarized electroluminescence based on organic light-emitting diodes. *Chem. Soc. Rev.* **49**, 1331–1343 (2020).
8. Z. Chen, C. Zhong, J. Han, J. Miao, Y. Qi, Y. Zou, G. Xie, S. Gong, C. Yang, High-performance circularly polarized electroluminescence with simultaneous narrowband emission, high efficiency, and large dissymmetry factor. *Adv. Mater.* **34**, e2109147 (2022).
9. Z.-P. Yan, L. Yuan, Y. Zhang, M.-X. Mao, X.-J. Liao, H.-X. Ni, Z.-H. Wang, Z. An, Y.-X. Zheng, J.-L. Zuo, A chiral dual-core organoboron structure realizes dual-channel enhanced ultrapure blue emission and highly efficient circularly polarized electroluminescence. *Adv. Mater.* **34**, e2204253 (2022).
10. N. Yu, F. Aieta, P. Genevet, M. A. Kats, Z. Gaburro, F. Capasso, A broadband, background-free quarter-wave plate based on plasmonic metasurfaces. *Nano Lett.* **12**, 6328–6333 (2012).
11. X. Tian, K. Shoyama, B. Mahlmeister, F. Brust, M. Stolte, F. Würthner, Naphthalimide-annulated [n] helicenes: Red circularly polarized light emitters. *J. Am. Chem. Soc.* **145**, 9886–9894 (2023).
12. M. Zeng, W. Wang, S. Zhang, Z. Gao, Y. Yan, Y. Liu, Y. Qi, X. Yan, W. Zhao, X. Zhang, N. Guo, H. Li, H. Li, G. Xie, Y. Tao, R. Chen, W. Huang, Enabling robust blue circularly polarized organic afterglow through self-confining isolated chiral chromophore. *Nat. Commun.* **15**, 3053 (2024).
13. P. Shen, S. Jiao, Z. Zhuang, X. Dong, S. Song, J. Li, B. Z. Tang, Z. Zhao, Switchable dual circularly polarized luminescence in through-space conjugated chiral foldamers. *Angew. Chem. Int. Ed. Engl.* **136**, e202407605 (2024).
14. Q. Zhang, T. Hernandez, K. W. Smith, S. A. H. Jebeli, A. X. Dai, L. Warning, R. Baiyasi, L. A. McCarthy, H. Guo, D.-H. Chen, J. A. Dionne, C. F. Landes, S. Link, Unraveling the origin of chirality from plasmonic nanoparticle-protein complexes. *Science* **365**, 1475–1478 (2019).
15. J. Cai, A.-A. Liu, X.-H. Shi, H. Fu, W. Zhao, L. Xu, H. Kuang, C. Xu, D.-W. Pang, Enhancing circularly polarized luminescence in quantum dots through chiral coordination-mediated growth at the liquid/liquid interface. *J. Am. Chem. Soc.* **145**, 24375–24385 (2023).
16. X. Yang, J. Lv, J. Zhang, T. Shen, T. Xing, F. Qi, S. Ma, X. Gao, W. Zhang, Z. Tang, Tunable circularly polarized luminescence from inorganic chiral photonic crystals doped with quantum dots. *Angew. Chem. Int. Ed. Engl.* **61**, e202201674 (2022).
17. G. Jang, D.-Y. Jo, S. Ma, J. Lee, J. Son, C. U. Lee, W. Jeong, S. Yang, J. H. Park, H. Yang, J. Moon, Core–shell perovskite quantum dots for highly selective room-temperature spin light-emitting diodes. *Adv. Mater.* **36**, 2309335 (2024).
18. Y. Wang, M.-S. Song, J. Zhao, Z. Li, T. Wang, H. Wang, H.-Y. Wang, Y. Wang, Chiral perovskite heterostructure films of CsPbBr3 quantum dots and 2D chiral perovskite with circularly polarized luminescence performance and energy transfer. *ACS Nano* **18**, 22334–22343 (2024).
19. C. Ye, J. Jiang, S. Zou, W. Mi, Y. Xiao, Core–shell three-dimensional perovskite nanocrystals with chiral-induced spin selectivity for room-temperature spin light-emitting diodes. *J. Am. Chem. Soc.* **144**, 9707–9714 (2022).
20. D. Han, X. Yang, J. Han, J. Zhou, T. Jiao, P. Duan, Sequentially amplified circularly polarized ultraviolet luminescence for enantioselective photopolymerization. *Nat. Commun.* **11**, 5659 (2020).
21. X. Gao, J. Wang, K. Yang, B. Zhao, J. Deng, Regulating the helical chirality of racemic polyacetylene by chiral polylactide for realizing full-color and white circularly polarized luminescence. *Chem. Mater.* **34**, 6116–6128 (2022).
22. X. Yang, M. Zhou, Y. Wang, P. Duan, Electric-field-regulated energy transfer in chiral liquid crystals for enhancing upconverted circularly polarized luminescence through steering the photonic bandgap. *Adv. Mater.* **32**, e2000820 (2020).
23. S. Liu, X. Liu, Y. Wu, D. Zhang, Y. Wu, H. Tian, Z. Zheng, W.-H. Zhu, Circularly polarized perovskite luminescence with dissymmetry factor up to 1.9 by soft helix bilayer device. *Matter* **5**, 2319–2333 (2022).
24. Z.-L. Gong, X. Zhu, Z. Zhou, S.-W. Zhang, D. Yang, B. Zhao, Y.-P. Zhang, J. Deng, Y. Cheng, Y.-X. Zheng, S.-Q. Zang, H. Kuang, P. Duan, M. Yuan, C.-F. Chen, Y. S. Zhao, Y.-W. Zhong, B. Z. Tang, M. Liu, Frontiers in circularly polarized luminescence: Molecular design, self-assembly, nanomaterials, and applications. *Sci. China Chem.* **64**, 2060–2104 (2021).
25. C. Yang, B. Wu, J. Ruan, P. Zhao, L. Chen, D. Chen, F. Ye, 3D-printed biomimetic systems with synergetic color and shape responses based on oblate cholesteric liquid crystal droplets. *Adv. Mater.* **33**, e2006361 (2021).
26. S. Zhu, Q. Meng, L. Wang, J. Zhang, Y. Song, H. Jin, K. Zhang, H. Sun, H. Wang, B. Yang, Highly photoluminescent carbon dots for multicolor patterning, sensors, and bioimaging. *Angew. Chem. Int. Ed. Engl.* **52**, 3953–3957 (2013).
27. Y. Shi, W. Su, Q. Teng, C. Li, T. Yuan, H. Xu, X. Song, Y. Han, S. Wei, Y. Zhang, X. Li, Y. Li, L. Fan, F. Yuan, Opportunity and application of chiral carbon dots. *Matter* **6**, 2776–2806 (2023).
28. Y. Shi, W. Su, F. Yuan, T. Yuan, X. Song, Y. Han, S. Wei, Y. Zhang, Y. Li, X. Li, L. Fan, Carbon dots for electroluminescent light-emitting diodes: recent progress and future prospects. *Adv. Mater.* **35**, e2210699 (2023).
29. F. Yuan, P. He, Z. Xi, X. Li, Y. Li, H. Zhong, L. Fan, S. Yang, Highly efficient and stable white LEDs based on pure red narrow bandwidth emission triangular carbon quantum dots for wide-color gamut backlight displays. *Nano Res.* **12**, 1669–1674 (2019).
30. Z. Wang, F. Yuan, X. Li, Y. Li, H. Zhong, L. Fan, S. Yang, 53% efficient red emissive carbon quantum dots for high color rendering and stable warm white-light-emitting diodes. *Adv. Mater.* **29**, 1702910 (2017).
31. F. Yuan, Z. Xi, X. Shi, Y. Li, X. Li, Z. Wang, L. Fan, S. Yang, Ultrastable and low-threshold random lasing from narrow-bandwidth-emission triangular carbon quantum dots. *Adv. Opt. Mater.* **7**, 1801202 (2019).
32. F. Yuan, S. Li, Z. Fan, X. Meng, L. Fan, S. Yang, Shining carbon dots: Synthesis and biomedical and optoelectronic applications. *Nano Today* **11**, 565–586 (2016).
33. Y. Shi, Y. Zhang, Z. Wang, T. Yuan, T. Meng, Y. Li, X. Li, F. Yuan, Z. Tan, L. Fan, Onion-like multicolor thermally activated delayed fluorescent carbon quantum dots for efficient electroluminescent light-emitting diodes. *Nat. Commun.* **15**, 3043 (2024).
34. T. Yuan, Q. Teng, C. Li, J. Li, W. Su, X. Song, Y. Shi, H. Xu, Y. Han, S. Wei, Y. Zhang, X. Li, Y. Li, L. Fan, F. Yuan, The emergence and prospects of carbon dots with solid-state photoluminescence for light-emitting diodes. *Mater. Horiz.* **11**, 102–112 (2023).
35. F. Yuan, Z. Wang, X. Li, Y. Li, Z. Tan, L. Fan, S. Yang, Bright multicolor bandgap fluorescent carbon quantum dots for electroluminescent light-emitting diodes. *Adv. Mater.* **29**, 1604436 (2017).
36. R. Chen, Z. Wang, T. Pang, Q. Teng, C. Li, N. Jiang, S. Zheng, R. Zhang, Y. Zheng, D. Chen, F. Yuan, Ultra-narrow-bandwidth deep-red electroluminescence based on green plant-derived carbon Dots. *Adv. Mater.* **35**, 2302275 (2023).
37. F. Yuan, T. Yuan, L. Sui, Z. Wang, Z. Xi, Y. Li, X. Li, L. Fan, Z. Tan, A. Chen, M. Jin, S. Yang, Engineering triangular carbon quantum dots with unprecedented narrow bandwidth emission for multicolored LEDs. *Nat. Commun.* **9**, 2249 (2018).
38. T. Yuan, F. Yuan, L. Sui, Y. Zhang, Y. Li, X. Li, Z. Tan, L. Fan, Carbon quantum dots with near-unity quantum yield bandgap emission for electroluminescent light-emitting diodes. *Angew. Chem. Int. Ed. Engl.* **62**, e202218568 (2023).
39. Z. Wang, F. Yuan, W. Sun, H. Shi, T. Hayat, A. Alsaedi, L. Fan, Z. Tan, Multifunctional p-type carbon quantum dots: A novel hole injection layer for high-performance perovskite light-emitting diodes with significantly enhanced stability. *Adv. Opt. Mater.* **7**, 1901299 (2019).
40. H. Jia, Z. Wang, T. Yuan, F. Yuan, X. Li, Y. Li, Z. Tan, L. Fan, S. Yang, Electroluminescent warm white light-emitting diodes based on passivation enabled bright red bandgap emission carbon quantum dots. *Adv. Sci.* **6**, 1900397 (2019).
41. F. Yuan, Y.-K. Wang, G. Sharma, Y. Dong, X. Zheng, P. Li, A. Johnston, G. Bappi, J. Z. Fan, H. Kung, B. Chen, M. I. Saidaminov, K. Singh, O. Voznyy, O. M. Bakr, Z.-H. Lu, E. H. Sargent, Bright high-colour-purity deep-blue carbon dot light-emitting diodes via efficient edge amination. *Nat. Photonics* **14**, 171–176 (2020).
42. C. Li, J. Li, Q. Teng, J. Li, F. Yuan, Single solid-state emissive carbon quantum dots for multicolor, bright and efficient electroluminescent light-emitting diodes. *Angew. Chem. Int. Ed. Engl.* **64**, e202419983 (2025).

43. M. Zhang, Q. Guo, Z. Li, Y. Zhou, S. Zhao, Z. Tong, Y. Wang, G. Li, S. Jin, M. Zhu, T. Zhuang, S.-H. Yu, Processable circularly polarized luminescence material enables flexible stereoscopic 3D imaging. *Sci. Adv.* **9**, eadi9944 (2023).
44. D. de Almeida Paula, E. M. F. Martins, N. de Almeida Costa, P. M. de Oliveira, E. B. de Oliveira, A. M. Ramos, Use of gelatin and gum arabic for microencapsulation of probiotic cells from lactobacillus plantarum by a dual process combining double emulsification followed by complex coacervation. *Int. J. Biol. Macromol.* **133**, 722–731 (2019).
45. B. A. San Jose, J. Yan, K. Akagi, Dynamic switching of the circularly polarized luminescence of disubstituted polyacetylene by selective transmission through a thermotropic chiral nematic liquid crystal. *Angew. Chem. Int. Ed. Engl.* **53**, 10641–10644 (2014).
46. X. Wang, B. Zhao, J. Deng, Liquid crystals doped with chiral fluorescent polymer: Multi-color circularly polarized fluorescence and room-temperature phosphorescence with high dissymmetry factor and anti-counterfeiting application. *Adv. Mater.* **35**, e2304405 (2023).
47. Y. Li, J. J.-Y. Suen, E. Prince, E. M. Larin, A. Klinkova, H. Thérien-Aubin, S. Zhu, B. Yang, A. S. Helmy, O. D. Lavrentovich, E. Kumacheva, Colloidal cholesteric liquid crystal in spherical confinement. *Nat. Commun.* **7**, 12520 (2016).
48. Y. Zhou, H. Li, T. Zhu, T. Gao, P. Yan, A Highly luminescent chiral tetrahedral $Eu_4L_4(L')_4$ cage: Chirality induction, chirality memory, and circularly polarized luminescence. *J. Am. Chem. Soc.* **141**, 19634–19643 (2019).
49. Y. Wang, N. Li, L. Chu, Z. Hao, J. Chen, J. Huang, J. Yan, H. Bian, P. Duan, J. Liu, Y. Fang, Dual enhancement of phosphorescence and circularly polarized luminescence through entropically driven self-assembly of a platinum(II) complex. *Angew. Chem. Int. Ed.* **63**, e202403898 (2024).
50. J. Zhang, L. Dai, A. M. Webster, W. T. K. Chan, L. E. Mackenzie, R. Pal, S. L. Cobb, G.-L. Law, Unusual magnetic field responsive circularly polarized luminescence probes with highly emissive chiral europium(III) complexes. *Angew. Chem. Int. Ed. Engl.* **60**, 1004–1010 (2021).
51. G. Long, C. Jiang, R. Sabatini, Z. Yang, M. Wei, L. N. Quan, Q. Liang, A. Rasmita, M. Askerka, G. Walters, X. Gong, J. Xing, X. Wen, R. Quintero-Bermudez, H. Yuan, G. Xing, X. R. Wang, D. Song, O. Voznyy, M. Zhang, S. Hoogland, W. Gao, Q. Xiong, E. H. Sargent, Spin control in reduced-dimensional chiral perovskites. *Nat. Photonics* **12**, 528–533 (2018).
52. J.-R. Jiménez, M. S. M. Poncet, S. Míguez-Lago, M. S. Stéphane Grass, J. Lacour, C. Besnard, J. M. Cuerva, A. G. Campaña, C. Piguet, Bright long-lived circularly polarized luminescence in chiral chromium(III) complexes. *Angew. Chem. Int. Ed. Engl.* **60**, 10095–10102 (2021).
53. Y. Shi, P. Duan, S. Huo, Y. Li, M. Liu, Endowing perovskite nanocrystals with circularly polarized luminescence. *Adv. Mater.* **30**, e1705011 (2018).
54. M.-M. Zhang, X.-Y. Dong, Z.-Y. Wang, X.-M. Luo, J.-H. Huang, S.-Q. Zang, T. C. W. Mak, Alkynyl-stabilized superatomic silver clusters showing circularly polarized luminescence. *J. Am. Chem. Soc.* **143**, 6048–6053 (2021).

Acknowledgments

Funding: This research was supported by the National Natural Science Foundation of China (22302012) (F.Y.), the Beijing Natural Science Foundation (2252037) (F.Y.), the National Key Research and Development Program of China (2023YFB3611800) (F.Y.), the Fundamental Research Funds for the Central Universities (2233300007) (F.Y.), and the National Science Fund for Excellent Young Scholars (Overseas) (F.Y.). **Author contributions:** Conceptualization: F.Y. and Jinsui L. Methodology: F.Y. and Jinsui L. Validation: Jinsui L., Q.Ta., Jinyang L., W.Q., C.L., Q.Te., Y.Y., Y.W., Y.C., Y.H., J.Z., and F.Y. Formal analysis: Jinsui L., Q.Ta., Jinyang L., W.Q., C.L., Q.Te., Y.Y., Y.W., Y.C., Y.H., J.Z., and F.Y. Investigation: Jinsui L., Q.Ta., Jinyang L., W.Q., C.L., Q.Te., Y.Y., Y.W., Y.C., Y.H., J.Z., and F.Y. Resources: F.Y. Data curation: F.Y. and Jinsui L. Writing—original draft: F.Y. and Jinsui L. Writing—review and editing: Jinsui L., Q.Ta., Jinyang L., W.Q., C.L., Q.Te., Y.Y., Y.W., Y.C., Y.H., J.Z., and F.Y. Visualization: Jinsui L., Q.Ta., Jinyang L., W.Q., C.L., Q.Te., Y.Y., Y.W., Y.C., Y.H., J.Z., and F.Y. Supervision: F.Y. Project administration: F.Y. Funding acquisition: F.Y. **Competing interests:** The authors declare that they have no competing interests. **Data and materials availability:** All data needed to evaluate the conclusions in the paper are present in the paper and/or the Supplementary Materials.

Submitted 12 October 2024
Accepted 14 April 2025
Published 16 May 2025
10.1126/sciadv.adt8219